Dyes and Pigments 143 (2017) 76–85

Contents lists available at ScienceDirect

Dyes and Pigments

journal homepage: www.elsevier.com/locate/dyepig

Organic dye doped nanoparticles with NIR emission and biocompatibility for ultra-deep *in vivo* two-photon microscopy under 1040 nm femtosecond excitation

Nuernisha Alifu [a], Lulin Yan [b], Hequn Zhang [a], Abudureheman Zebibula [c], Zhenggang Zhu [d], Wang Xi [e], Anna Wang Roe [e], Bin Xu [b, **], Wenjing Tian [b], Jun Qian [a, *]

[a] State Key Laboratory of Modern Optical Instrumentations, Centre for Optical and Electromagnetic Research, JORCEP (Sino-Swedish Joint Research Center of Photonics), Zhejiang University, Hangzhou, 310058, China
[b] State Key Lab of Supramolecular Structure and Materials, Jilin University, Changchun, 130012, China
[c] Department of Urology, Sir Run-Run Shaw Hospital, College of Medicine, Zhejiang University, Hangzhou, 310016, China
[d] Department of Neurobiology, Key Laboratory of Medical Neurobiology of Ministry of Health of China, Zhejiang Province Key Laboratory of Neurobiology School of Medicine, Zhejiang University, Hangzhou, Zhejiang, 310058, China
[e] Interdisciplinary Institute of Neuroscience and Technology (ZIINT), Zhejiang University, Hangzhou, Zhejiang, 310020, China

ARTICLE INFO

Article history:
Received 10 November 2016
Received in revised form
12 April 2017
Accepted 12 April 2017
Available online 14 April 2017

Keywords:
Organic dye nanoparticles
NIR fluorescence
Two-photon fluorescence
In vivo
Brain imaging

ABSTRACT

Nanoparticle-assisted near-infrared (NIR) bioimaging and two-photon fluorescence microscopy (TPFM) are two important technologies in biophotonic research. In this work, we synthesize the dye named 2-(4-bromophenyl)-3-(4-(4-(diphenylamino)styryl)phenyl)fumaronitrile (TPABDFN), which had a large two-photon absorption cross-section and bright NIR emission. The dyes were then encapsulated with poly(styrene-*co*-maleic anhydride) (PSMA), forming fluorescent nanoparticles. The TPABDFN-PSMA nanoparticles possessed high chemical and optical stability, good biocompatibility, as well as large two-photon absorption cross-section (5.56×10^5 GM). Furthermore, we combined NIR bioimaging and TPFM together, and utilized TPABDFN-PSMA nanoparticles as fluorescent contrast agents for two-photon excited NIR microscopic imaging, with a 1040 nm-femtosecond laser. *In vivo* angiography of mice ear and brain was performed. Due to the deep penetration capability of both 1040 nm-excitation and NIR emission light, a very large *in vivo* microscopic imaging depth (~1.2 mm) was achieved. NIR emissive and biocompatible TPABDFN-PSMA nanoparticles have great potential in disease diagnosis and clinical therapies, where deep-tissue imaging is required.

1. Introduction

Fluorescence imaging occupies a very significant position in the field of life science and biomedicine [1], since it can offer high spatial resolution [2,3] and sensitivity [4] to bio-samples. Deep-tissue fluorescence imaging has attracted great attention, as it has been widely used for functional brain imaging [5], sentinel lymph node mapping [6], as well as tumor targeting [6] *etc*, which are essential to clinical diagnosis and biomedical research.

The focusing ability and penetration depth of a light beam are limited by the optical absorption and scattering of biological tissue. Thus, the depth of fluorescence imaging is usually limited, and becomes a bottleneck in practical biomedical applications. Near-infrared (NIR) fluorescence imaging and two-photon fluorescence microscopy (TPFM) are two kinds of deep-tissue fluorescence imaging approaches, since they overcome the obstacle arose from tissue absorption and scattering to some extent.

The emission signal in NIR fluorescence imaging is usually located in the spectral region of 700–900 nm [7]. In this region, light absorption of water is very small, and light scattering in tissue is not so distinct. Thus, the penetration capability of emission signals in tissues can be greatly enhanced, and this is the main reason why NIR fluorescence imaging can realize a large imaging depth. However, NIR fluorescence imaging is usually performed on a whole-body *in vivo* imaging experiment and spatial resolution of this imaging mode is usually limited. TPFM is another alternative for deep-tissue bioimaging. Different from NIR fluorescence imaging, the

* Corresponding author.
** Corresponding author.
E-mail addresses: xubin@jlu.edu.cn (B. Xu), qianjun@zju.edu.cn (J. Qian).

http://dx.doi.org/10.1016/j.dyepig.2017.04.017
0143-7208/

femtosecond (fs) excitation wavelength in most TPFM located in 700–900 nm, which is very helpful to increase the penetration depth of excitation light. Moreover, due to the nonlinear excitation mode of two-photon fluorescence, the region of bio-samples outside the beam focus cannot be excited, and it is able to reduce the possibility of photobleaching, as well as improve the spatial resolution of imaging. However, the emission signal of TPFM is usually in the visible light region, and it has relatively large loss during the transmission in biological tissues, which further limits the detection efficiency and affects the imaging depth. Thus, it is necessary to combine the advantages of both NIR imaging and TPFM, and establish a new fluorescence imaging technology called two-photon excited NIR fluorescence microscopy (TPNIRFM), in order to further increase the imaging depth, as well as spatial resolution.

Bioimaging research has promoted the development of fluorescence nanomaterials and recently a variety of fluorescent nanoparticles have been widely used in NIR fluorescence bioimaging and TPFM, such as quantum dots (QDs) [8,9], upconversion nanoparticles (UCNPs) [10,11]. QDs have the advantages of high brightness, tunable absorption and emission spectra [12,13]. However, QDs composed of heavy metal ions have potential toxicity [14], and they are usually excreted slowly from the animal body through the reticuloendothelial system [15]. The absorption and emission spectra of UCNPs are sharp and tunable [16,17], and UCNPs assisted bioimaging has a high signal to noise ratio. However, the long luminescence lifetime of UCNPs restricts the speed of bioimaging, especially in scanning microscopy [18].

In this paper, we prepared an organic fluorescent dye named 2-(4-bromophenyl)-3-(4-(4-(diphenylamino) styryl) phenyl) fumaronitrile (TPABDFN), which had a donor-acceptor (D-A) structure. The long π-conjugation length endowed the organic dye with two important features, which are long-wavelength (NIR) emission and large two-photon absorption cross-section, and it met well with the requirement of TPNIRFM. The commercially available polymer, poly(styrene-*co*-maleic anhydride) (PSMA) was used to encapsulate TPABDFN, to form NIR emissive fluorescent nanoparticles. By changing the weight ratio of TPABDFN to PSMA, the emission quantum yield, as well as the peak emission wavelength of TPABDFN-PSMA nanoparticles, could be easily tuned. Long-chain PEG molecules were further conjugated with TPABDFN-PSMA nanoparticles, which could avoid the capture of nanoparticles by the reticuloendothelial/degradation system, and increase their circulation time in live mice body. Chemically stable and biocompatible TPABDFN-PSMA nanoparticles were further used as fluorescent contrast agents for TPNIRFM imaging, under the excitation of a 1040 nm-fs laser. The 1040 nm-fs excitation light could penetrate deeper and focus better [19] in the biological tissue than the 700-900 nm-fs laser beam, while the latter one has been widely utilized as the excitation source in commercial TPFM imaging systems. In addition, the 1040 nm-fs excitation light could be easily filtered away from the emission signals (600–900 nm) of TPABDFN-PSMA nanoparticles. The NIR fluorescent nanoparticles were then used to stain cancer cells, and *in vitro* TPNIRFM cell imaging was performed. The TPABDFN-PSMA-PEG nanoparticles were intravenously injected into mice, and *in vivo* ear and brain angiography of live mice was realized. Due to the deep penetration and good focusing capability of 1040 nm-fs excitation, as well as the low loss of NIR emission in biological tissue, the imaging depth in *in vivo* TPNIRFM of mice brain could reach as large as 1200 μm.

2. Experimental

2.1. Materials

2-(4-Bromophenyl) acetonitrile, iodine, sodium methoxide, $Ph_3P^+CH_3Br^-$, t-BuOK, 4-(*N,N*-diphenylamino) benzaldehyde, $Pd(OAc)_2$, $AgCO_3$, diethyl ether were purchased from J&K Scientific Ltd. Poly(styrene-*co*-maleic anhydride) (PSMA), methoxypolyethylene glycol amine (mPEG-NH_2), 1-ethyl-3-(3-dimethylaminopropyl) carbodiimide hydrochloride (EDC), 1-hydroxy-2,5-pyrrolidinedione (NHS) were purchased from Sigma.

2.2. Methods

The NMR (^{1}H NMR and ^{13}C NMR) spectra of TPABDFN were recorded using a Bruker Avance III 500 instrument at 500 MHz. The mass spectra of TPABDFN were recorded on an Agilent 1100 LC-MS system. The FTIR spectra of TPABDFN were measured by a Fourier Transform Infrared Spectrometer (FTIR) (Bruker, IFS66V). The DSC curves of the TPABDFN were measured by a Thermal Analysis system (Perkin-Elmer) at heating rate of 10 K/min and nitrogen flow rate of 80 mL/min. The self-assembly process was completed using a bath sonicator (Bransonic, MH 2510). TEM images of TPABDFN-PSMA and TPABDFN-PSMA-PEG nanoparticles were captured by a JEOL JEM-1200EX microscope operated at 160 kV. UV-vis absorption spectra of TPABDFN, TPABDFN-PSMA and TPABDFN-PSMA-PEG nanoparticles were recorded with a Shimadzu UV-3600 UV-vis spectrophotometer. Photoluminescence (PL) spectra of TPABDFN, TPABDFN-PSMA and TPABDFN-PSMA-PEG nanoparticles were collected on a Shimadzu RF-5301 PC spectrophotometer. PL efficiency of solid state TPABDFN was measured using an integrating sphere (C-701, Labsphere Inc.) equipped with a 365 nm Ocean Optics LLS-LED as the excitation source. The DLS measurements of TPABDFN-PSMA and TPABDFN-PSMA-PEG nanoparticles were performed using a Malvern Zetasizer Nano ZS size analyser at room temperature. Two-photon fluorescence spectra of TPABDFN-PSMA nanoparticles, which were excited by a 1040 nm-fs laser [from an amplified output of a large-mode-area ytterbium-doped photonic crystal fiber (PCF) oscillator (150 fs, 50 MHz)] were measured by a home-built system and collected with an optical fiber spectrometer (PG2000, Ideaoptics Instruments).

2.3. Synthesis of 2,3-bis(4-bromophenyl) fumaronitrile (1)

2-(4-Bromophenyl) acetonitrile (5.00 g, 25.5 mmol) and iodine (6.57 g, 25.5 mmol) were dissolved in dry diethyl ether (100 mL). Sodium methoxide (2.89 g, 5.3 mmol) in methanol solution (8.68 g, 14.61 mL) was added slowly (over a period of 30 min) into the reaction solution at a dry-ice temperature, under an argon atmosphere. The reaction solution was allowed to warm up by replacing the dry-ice bath with an ice–water bath before the temperature rose above 0 °C. The reaction solution was further stirred for another 3–4 h, and the reaction was then quenched with 5% hydrochloric acid. After stirring for another 12 h, the resulting solution was filtered to isolate the solid, which was rinsed with cold methanol and water. The resulting mixture was then dried further reaction. Compound 1 (3.11 g, 63% yield); ^{1}H NMR ($CDCl_3$, 500 MHz) δ [ppm]: 7.67–7.72 (m, 8H, 1-benzene).

2.4. Synthesis of 2-(4-bromophenyl)-3-(4-(4-(diphenylamino) styryl) phenyl) fumaronitrile (TPABDFN)

$Ph_3P^+CH_3Br^-$ (2.31 g, 6.5 mmol) and t-BuOK (0.89 g, 8 mmol) were dissolved in dry tetrahydrofuran (80 mL) at an ice temperature, under an argon atmosphere. The reaction solution was stirred for 1 h, and 4-(*N, N*-diphenylamino) benzaldehyde (1.36 g, 5 mmol) in dry tetrahydrofuran (40 mL) was added slowly (over a period of 30 min) into the reaction solution under an argon atmosphere. The reaction solution was further stirred for 12 h. The resulting solution was filtered to isolate the solid, which was rinsed with

tetrahydrofuran. The organic solution was further purified by the column chromatography (silica gel; DCM: n-hexane = 1: 3). Compound 2 was obtained as a white solid in 69% yield. Compound 1 (200 mg, 0.52 nmol), Compound 2 (140 mg, 0.52 mmol), $Pd(OAc)_2$ (6 mg, 0.026 mmol), and Ag_2CO_3 (85 mg, 0.31 mmol) were dissolved in toluene (10 mL) at a 50 mL Schlenk tube. The reaction solution was further stirred at 100 °C for 18 h. The resulting solution was filtered to isolate the solid, which was rinsed with DCM. The organic solution was purified by the column chromatography (silica gel; DCM: n-hexane = 2: 1). TPABDFN was obtained as a red solid in 62.8% yield. The melting point of TPABDFN is 201.5 °C; IR (KBr, cm^{-1}) wavenumber: 4000, 3500, 3000, 2500, 2000, 1500, 1000, 500; ^1H NMR (DMSO, 500 MHz) δ [ppm]: 7.82 (ddd, J = 13.8, 8.6, 6.0 Hz, 8H), 7.55 (d, J = 8.7 Hz, 2H), 7.43 (s, 1H), 7.39 (s, 1H), 7.33 (dd, J = 8.3, 7.5 Hz, 4H), 7.22 (s, 1H), 7.19 (s, 1H), 7.11–7.03 (m, 6H), 6.96 (d, J = 8.6 Hz, 2H). ^{13}C NMR (126 MHz, $CDCl_3$) δ [ppm]: 148.50, 147.55, 141.94, 132.82, 131.80, 131.43, 130.51, 130.44, 130.21, 129.62, 129.39, 128.08, 127.07, 126.52, 125.94, 125.23, 125.09, 123.68, 123.20, 122.53, 116.98, 116.71, 77.51, 77.25, 77.00, 0.24. HRMS: m/z (EI) found $[M+H]^+$ 579.1908; molecular formula $C_{36}H_{24}BrN_3$ requires $[M+H]^+$ 579.5000.

2.5. Synthesis of TPABDFN-PSMA nanoparticles

TPABDFN-PSMA nanoparticles were prepared by using a self-assembly method as described previously [20,21]. Typically, TPABDFN (10 mg) was added in a 10 mL volumetric flask, and then diluted with THF to make stock solution A (1 mg/mL). Stock solution B containing PSMA (1 mg/mL) was prepared with the similar method. 200 μL stock solution B and stock solution A with different volumes (200 μL, 100 μL, 50 μL, 33.3 μL, and 25 μL, 20 μL, and 8 μL) were mixed to produce a solution mixture. After dilution to 1 mL with THF, the mixture was quickly added to 5 mL MilliQ water under the ultrasonication to form TPABDFN-PSMA nanoparticles. During the reaction, the maleic anhydride units in PSMA molecules were hydrolyzed in the aqueous environment, generating carboxyl groups on the nanoparticles. The THF was completely removed under a steady stream of nitrogen and the nanoparticles were filtered with a 0.22 μm filter. The dispersions of TPABDFN-PSMA nanoparticles were clear and stable for months without signs of aggregation.

2.6. Synthesis of TPABDFN-PSMA-PEG nanoparticles

TPABDFN-PSMA-PEG nanoparticles were synthesized by using the EDC-catalyzed reaction between the carboxyl groups on the surface of TPABDFN-PSMA nanoparticles and the amine groups on mPEG-NH_2. The TPABDFN-PSMA nanoparticles were concentrated to 10 mL (220 μg/mL of TPABDFN), followed by the addition of 200 μL of EDC (1 mmol) and 200 μL of NHS (1 mmol) for 10-min-reaction. 20 mg mPEG-NH_2 (1 mmol) was then added into the mixed solution to react for 2 h at room temperature. The resulting mixture was kept rotating for 6 h at room temperature. The TPABDFN-PSMA-PEG nanoparticles were purified by dialyzing the mixed solution against deionized water for 3 days. Finally, the aqueous dispersion of TPABDFN-PSMA-PEG nanoparticles was concentrated to 10 mL, and the final concentration was calibrated according to its absorption spectrum.

2.7. Cell viability analysis

The cytotoxicity of TPABDFN-PSMA nanoparticles towards HeLa cells was evaluated by following the instructions of cell counting kit-8 (CCK-8). 5000 cells/well in a 100 μL suspension were incubated in 96-well plates for 24 h. Then, 100 μL fresh culture medium containing TPABDFN-PSMA nanoparticles with various concentrations (ranging from 0 to 25.6 μg/mL) was added into each well. After incubation for 24 h, the culture medium was removed and the cell well was washed three times with PBS. In the end, 100 μL culture medium containing CCK-8 (10%) was added into each well for 2 h, and the absorbance at 450 nm was measured with a microplate reader (Thermo, USA).

2.8. Animal preparation

All the animal experiments were performed strictly in compliance with the requirements and guidelines of the Institutional Ethical Committee of Animal Experimentation of Zhejiang University. The ICR mice (~18 g, female) and nude mice (18–20 g, male) were obtained from the Laboratory Animal Center of Zhejiang University (Hangzhou, China). The mice were housed in cages at 24 °C with a 12 h light/dark cycle and were fed with standard laboratory water and chow.

2.9. Histology

TPABDFN-PSMA-PEG nanoparticles (in 300 μL 1 × PBS, 0.125 mg/mL) were intravenously injected into the ICR mice. 24, 48, and 72 h later, both the experimental mice (with the injection of nanoparticles), and control mice (without the injection of nanoparticles), were sacrificed. Their major organs (heart, liver, lung, kidney, brain and spleen) were removed for histological analysis. Tissue samples were harvested and fixed in 4% paraformaldehyde overnight at 4 °C. The samples were embedded in paraffin, sectioned, and stained with hematoxylin and eosin (H&E). The histological sections were imaged under an inverted optical microscope (40×).

2.10. In vivo TPNIRFM imaging of ear blood vessels

300 μL PBS (1×) solution of TPABDFN-PSMA- PEG nanoparticles (0.125 mg/mL) were intravenously injected into the ICR mice. The mice in the control group were intravenously injected with 300 μL PBS (1×). The mice were anesthetized and placed on a Petri dish with one ear attached to the coverslip, and put under the aforementioned two-photon fluorescence scanning microscope for imaging. The 1040 nm fs laser beam was focused by the water-immersed objective lens (25×/1.05, Olympus) onto the earlobe immersed in water. The two-photon fluorescence signals of nanoparticles (from the mouse ear) passed through a 590 nm long pass filter, and collected by a photomultiplier tube (PMT) via non-descanned detection (NDD) mode.

2.11. In vivo TPNIRFM imaging of brain blood vessels

A cranial window microsurgery on the mouse brain was performed. Briefly, mice were anesthetized and a small piece of skull was excised using a dental drill. The surgery was operated under sterile conditions to avoid infections and any damage to the dura mater, as well as ensure that the mice could live well during the whole imaging process. The mice were then intravenously injected with 300 μL PBS (1×) solution of TPABDFN-PSMA-PEG nanoparticles, and placed under the aforementioned two-photon fluorescence scanning microscope after anesthetized. For the description of the immobilization of mice's heads and how the objective of the upright two-photon scanning microscope was arranged to contact the mice brain, we refer to our previous work [22]. The two-photon fluorescence signals of nanoparticles (from the mouse brain) passed through a 590 nm long pass filter, and collected by a photomultiplier tube (PMT) via non-descanned detection (NDD) mode.

2.12. Measurements of two-photon absorption cross-section

Two-photon action cross-section ($\eta\delta$) is the product of two-photon cross-section (δ) and fluorescence quantum yield (η), and it is a parameter describing how bright a fluorophore is under two-photon excitation. Herein, the two-photon cross-sections (δ) of TPABDFN-PSMA nanoparticles was measured, via a two-photon induced fluorescence method [19,23]. The amplified output of the large-mode-area ytterbium-doped photonic crystal fiber (PCF) oscillator (1040 nm, 150 fs, 50 MHz) was adopted for the measurement of δ at 1040 nm. The fs laser beam was focused onto the sample in a cuvette by a lens (f = 40 mm), and the focus was near the edge of the cuvette to minimize self-absorption of two-photon fluorescence signal by the sample. The signal from the sample was collected by an objective (20 ×, NA = 1.00), which was perpendicular to the laser beam propagation direction, filtered by a 775 nm short-pass optical filter, and directed into a spectrometer (PG2000, Ideaoptics Instruments). Rhodamine B (RhB) in methanol was used as reference [24].

The two-photon cross-sections of TPABDFN-PSMA nanoparticles was calculated according to the following equation [25]:

$$\frac{\delta_1}{\delta_2} = \frac{F_1 \eta_2 c_2 n_2}{F_2 \eta_1 c_1 n_1}$$

where δ is the two-photon absorption cross-section, F is the two-photon fluorescence intensity, η is the fluorescence quantum yield (QY), c is the molar concentration, n is the refractive index of the solvent, and the subscripts 1 and 2 represent the sample (TPABDFN-PSMA nanoparticles in water) and the reference (RhB in methanol).

3. Results and discussion

3.1. Synthesis and characterizations of TPABDFN

TPABDFN was designed based on the molecules reported by X. Shen et al. [20] and X. Han et al. [21]. The molecules described in the work by X. Han et al., has a simpler structure and brighter NIR emission, as well as simple synthesis. Thus, triphenylamine with a twisted structure was chosen as the donor part in the TPABDFN molecule, and it was connected with the fumaric acid nitrile via a double bond. The reason for introducing a double bond was to increase the π-conjugation length of the molecule, which was helpful to obtain longer-wavelength (NIR) emission and larger two-photon absorption cross-section. According to the synthetic routes shown in Fig. 1a TPABDFN was obtained as a red solid in 62.8% yield. The purified product was characterized using standard spectroscopic methods. Examples of its ^{1}H NMR and ^{13}C NMRspectra are shown in Figs. S1–S4 shows the high-resolution mass spectrum of TPABDFN molecule. Fig. S6 shows the FTIR spectrum of the TPABDFN powder. Fig. S5 shows the DSC curve of the TPABDFN powder. According to Figs. S2–S7, we demonstrated the complete characterization of TPABDFN molecular synthesis. Fig. 1b shows the fluorescence spectra of TPABDFN in the solid state (PL $\lambda_{peak} \approx 800$ nm) and in tetrahydrofuran (THF) solution (PL $\lambda_{peak} \approx 710$ nm). The quantum yield (QY) of TPABDFN dissolved in THF and in solid state were 1.03% and 5.9%, respectively. According to the absorption spectra in Fig. 1b, TPABDFN in both solution and solid state had absorption peaks in the blue spectral region, which were mainly due to the π-π* transition [26].

TPABDFN in THF solution exhibited a broader fluorescence emission spectrum, as well as lower fluorescence efficiency. Since the triphenylamine groups in the TPABDFN molecules could vibrate and rotate freely in THF solution, they consumed the excited state energy by non-radiative transition, which reduced the fluorescence efficiency and lifetime, as well as broadened the emission spectrum [27,28]. In addition, the Stokes-shift of TPABDFN in THF solution was about 330 nm, which means that the structure of the ground state and excited state were significantly different. The fumaric acid nitrile group inside the TPABDFN molecule had two cyano groups, which had strong electron-withdrawing ability. The N atom in the triphenylamine group had lone pair of electrons, which was connected to the fumaric acid nitrile group via double bond, forming a strong donor group. The whole TPABDFN molecule was a donor-acceptor structure, which could help to reduce the orbital overlap of the excited state and form a charge transfer state.

From the theoretical calculation results showed in Fig. S7, it can be found that at the optimized gaseous state structures, the HOMO (Highest Occupied Molecular Orbital) basically focused on the triphenylamine unit, while for LUMO (Lowest Unoccupied Molecular Orbital), electron cloud all distributed in the fumaric acid nitrile unit. The corresponding energy levels of the HOMO and LUMO were respectively −5.07 eV and −2.83 eV (bandgap was 2.24 eV). The results of the ground state structure indicate that the TPABDFN molecule had unidirectional dipole (Dipole moment = 5.79 debye), and the dipole moment direction was from the fumaric acid nitrile unit to the triphenylamine unit (obtained by theoretical simulation showed in Fig. S8). The solid state TPABDFN had a stronger fluorescence emission and the emission had an apparent blue-shift compared with that of TPABDFN in THF solution. This is due to the reason that the structure of solid state TPABDFN is more distorted than that of TPABDFN in THF solution [29].

3.2. Synthesis and characterizations of TPABDFN-PSMA nanoparticles

TPABDFN molecules were encapsulated with PSMA polymer

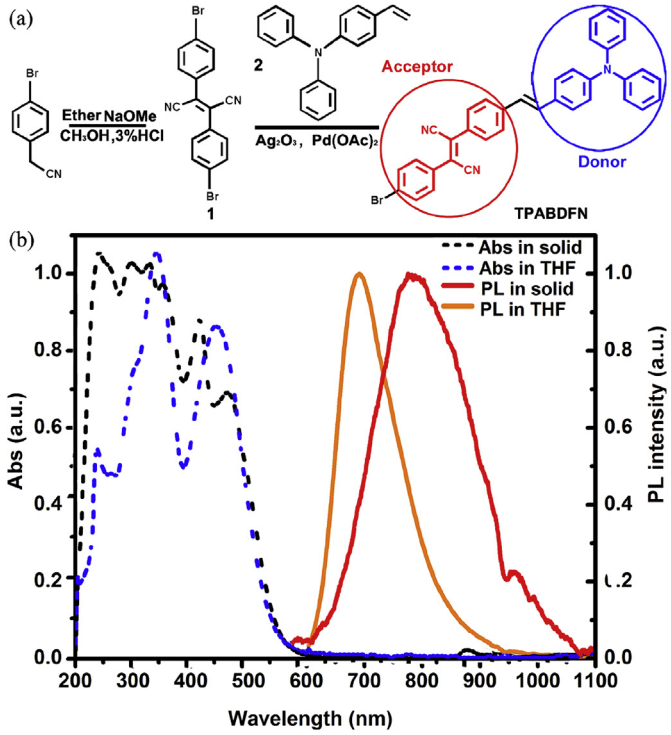

Fig. 1. Preparation and optical characterization of TPABDFN. (a) Synthetic routes to TPABDFN. (b) Absorption (black dotted line) and fluorescence (red line) spectra of TPABDFN in solid state. Absorption (blue dotted line) and fluorescence (orange line) spectra of TPABDFN in THF. $\lambda_{excitation}$ = 380 nm. (For interpretation of the references to colour in this figure legend, the reader is referred to the web version of this article.)

(Fig. 2a) at a weight ratio (TPABDFN: PSMA) of 1:25. The morphology of the TPABDFN-PSMA nanoparticles was characterized by TEM (Fig. 2c), and the average size of nanoparticles was about 40 nm. Fig. 2d shows the absorption and fluorescence spectra of TPABDFN-PSMA nanoparticles in aqueous dispersion, and the absorption peak was at 480 nm while the fluorescence peak was at

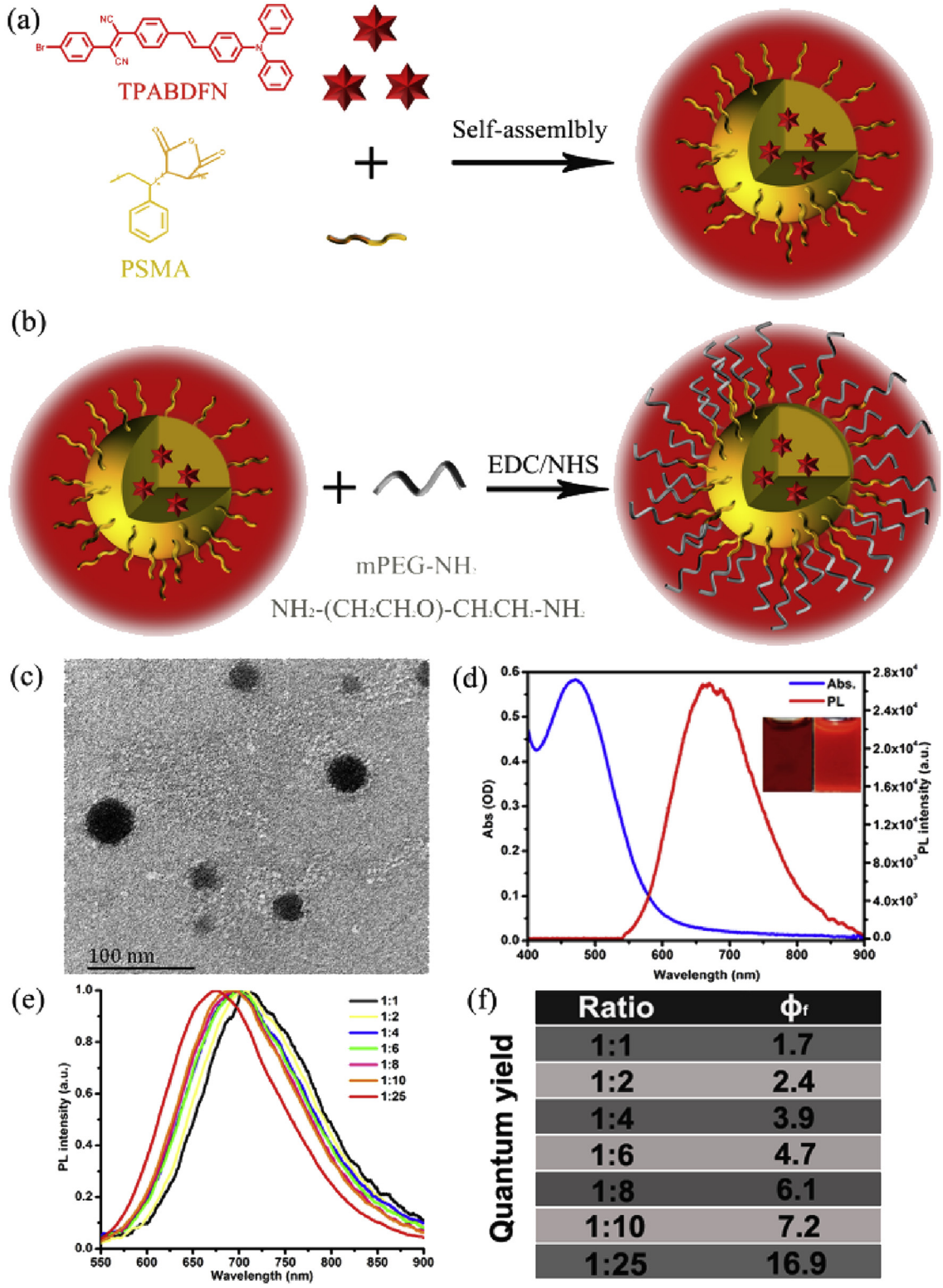

Fig. 2. (a) An illustration of the fabrication of TPABDFN-PSMA nanoparticles (TPABDFN: PSMA = 1: 25). (b) An illustration of the fabrication of TPABDFN-PSMA-PEG nanoparticles (TPABDFN: PSMA = 1: 25). (c) A TEM image of TPABDFN-PSMA nanoparticles, scale bar: 100 nm; (d) Absorption (blue line) and fluorescence spectra (red line) of TPABDFN-PSMA nanoparticles. Inset: bright filed (under daylight lamp) and fluorescence (under UV lamp) photographs of TPABDFN-PSMA nanoparticles. (e) Normalized fluorescence spectra of TPABDFN-PSMA nanoparticles with different weight ratios (TPABDFN: PSMA). (f) Emission quantum yield of TPABDFN-PSMA nanoparticles with different weight ratios (TPABDFN: PSMA), $\lambda_{excitation}$ = 380 nm. (For interpretation of the references to colour in this figure legend, the reader is referred to the web version of this article.)

678 nm. Compared with the emission peak (710 nm) of TPABDFN in solid state, the emission of TPABDFN-PSMA nanoparticles in aqueous dispersion was blue-shifted. This is because the benzene rings of the PSMA inserted among TPABDFN molecules and increased their molecular spacing, as well as weakened the interaction among neighboring molecules.

Furthermore, TPABDFN-PSMA nanoparticles with different weight ratios (TPABDFN: PSMA) were synthesized, respectively. It was found that the emission wavelength of TPABDFN-PSMA nanoparticles was tunable when changing the weight ratio of TPABDFN and PSMA. For example, when the amount of TPABDFN was kept constant and the amount of PSMA was increased (e.g., TPABDFN: PSMA = 1:1, 1:2, 1:4, 1:6, 1:8, 1:10, 1:25), the peak fluorescence wavelength of TPABDFN-PSMA nanoparticles gradually blue-shifted, from 706 nm to 676 nm (Fig. 2e). This is because when increasing the amount of PSMA, more benzene rings of the PSMA inserted among TPABDFN molecules and the interaction among neighboring TPABDFN molecules was weakened more. In addition, when changing the weight ratio of TPABDFN and PSMA in TPABDFN-PSMA nanoparticles, the emission QY of nanoparticles were also affected. As shown in Fig. 2f, the QY could be tuned from 1.7% to 16.9%, when the weight ratio (TPABDFN: PSMA) changed from 1:1 to 1:25.

3.3. PEG grafting on TPABDFN-PSMA nanoparticles

PEG is a biocompatible polymer and it can stablize TPABDFN-PSMA nanoparticles as well as improve the long circulation of nanoparticles in an animal body during *in vivo* experiments [30]. mPEG-NH_2 molecules were covalently conjugated with TPABDFN-PSMA nanoparticles (TPABDFN: PSMA = 1:25), as shown in Fig. 2b. The TPABDFN-PSMA-PEG nanoparticles were water dispersible, and could keep stable for several months. Nanoparticles were further characterized by TEM images (insets in Fig. S9a and b) and dynamic light scattering (DLS, Fig. S9a and b). Before PEG grafting, TPABDFN-PSMA nanoparticles had an average hydrodynamic size of ~71.29 nm (Fig. S9a), while after PEG grafting, the average hydrodynamic size of TPABDFN-PSMA-PEG nanoparticles was ~110.06 nm (Fig. S9b). Furthermore, even after PEG modification, the absorption spectrum of TPABDFN-PSMA-PEG nanoparticles was similar with that of TPABDFN-PSMA nanoparticles, and had no distinct shift of the peak fluorescence wavelength (Fig. S10). The above results illustrated that PEG molecules have been successfully grafted on the surface of TPABDFN-PSMA nanoparticles without any aggregation.

3.4. Chemical stability

In order to understand the chemical stability of TPABDFN-PSMA nanoparticles, the fluorescence intensities of TPABDFN-PSMA nanoparticles were recorded in, with pH values varying from 1 to 12, for 24 h. As shown in Fig. 3a, the variations of emission intensities of TPABDFN-PSMA nanoparticles were less than 10% in all experimental conditions (normalized by the emission intensity at pH = 7, 0 h), indicating that TPABDFN-PSMA nanoparticles could be dispersed uniformly and stably in various chemical environments for at least 24 h.

3.5. Toxicity of TPABDFN-PSMA nanoparticles

Fig. 3b showed the relative viabilities of HeLa cells treated with TPABDFN-PSMA-PEG nanoparticles after 24 h. The cells treated with TPABDFN-PSMA-PEG nanoparticles maintained very high viabilities, and it was still larger than 95% (Fig. 3b) even when the

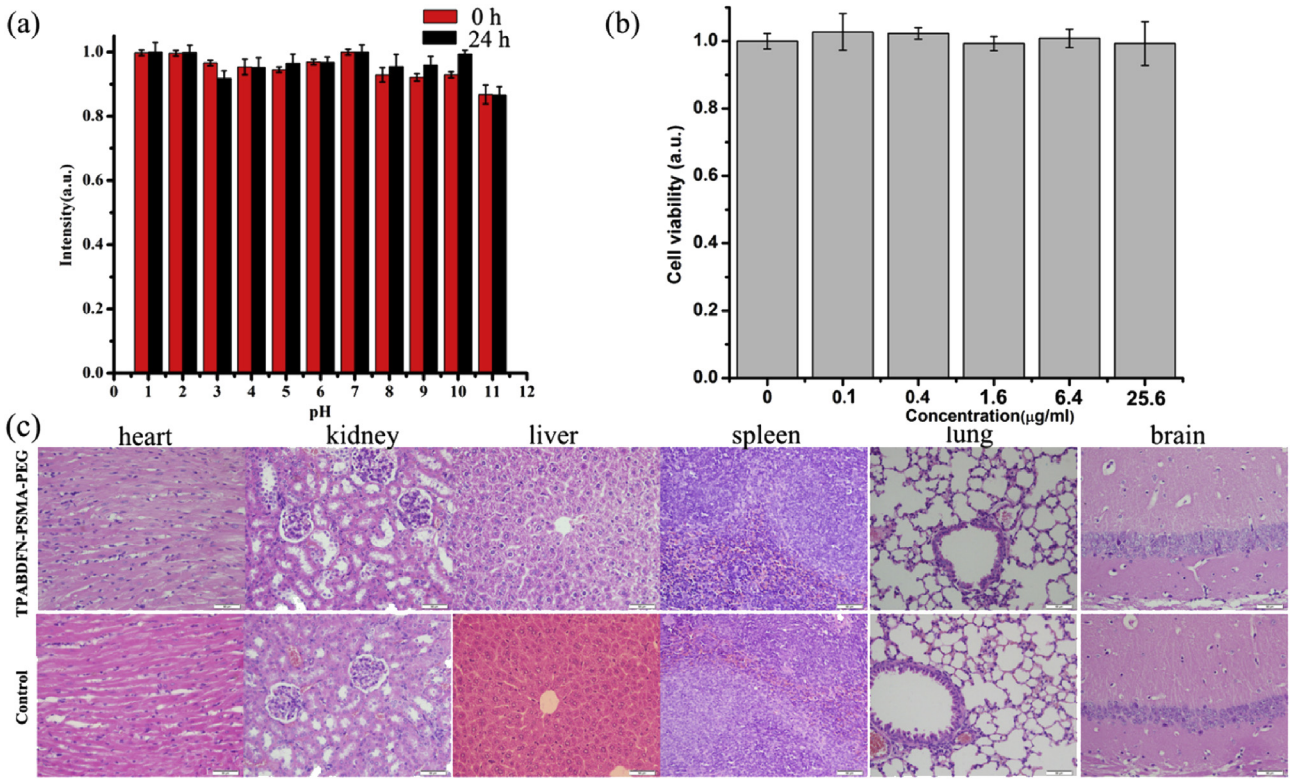

Fig. 3. (a) Emission intensity comparison between freshly synthesized TPABDFN-PSMA nanoparticles and TPABDFN-PSMA nanoparticles after a 24 h-treatment with different pH values (1–12). (b) Viability of HeLa cells after incubation with TPABDFN-PSMA-PEG nanoparticles with various concentrations for 24 h. (c) Microscopic images of tissue sections from a mouse receiving no injection (down) and a mouse injected with TPABDFN-PSMA-PEG nanoparticles for 24 h (up). Scale bar: 50 μm.

concentration of TPABDFN-PSMA-PEG nanoparticles was as high as 0.0256 mg/mL. Furthermore, *in vivo* biocompatibility of TPABDFN-PSMA-PEG nanoparticles was assessed by using a histopathology examination. 24 h post-administration of TPABDFN-PSMA-PEG nanoparticles, mice had no inflammation or abnormalities on their major organs (hear, liver, spleen, lung, kidney and brain, Fig. 3c), during the accumulation of TPABDFN-PSMA-PEG nanoparticles via the blood circulation, suggesting that TPABDFN-PSMA-PEG nanoparticles were highly biocompatible. Similar results were observed in the organs of mice, which were harvested 48 and 72 h post the administration of TPABDFN-PSMA-PEG nanoparticles (Fig. S11). The low cytotoxicity and high biocompatibility of TPABDFN-PSMA-PEG nanoparticles make them excellent optical probes for various *in vitro* and *in vivo* bioimaging applications.

3.6. Two-photon fluorescence properties of TPABDFN-PSMA nanoparticles

A 1040 nm-fs laser [from an amplified output of a large-mode-area ytterbium-doped photonic crystal fiber (PCF) oscillator (150 fs, 50 MHz)] was used for two-photon study of aqueous dispersion of TPABDFN-PSMA nanoparticles in a cuvette (Fig. S14). As shown in Fig. 4a, the two-photon fluorescence spectrum of nanoparticles ranged from 500 to 950 nm (with the maximum located at 700 nm). The envelope of fluorescence spectrum was very similar to that under one-photon excitation (Fig. 2d). That means in both one-photon (Fig. S13) and two-photon processes (Fig. 4c), the excited TPABDFN-PSMA nanoparticles were finally relaxed to the same lowest excited electronic-vibrational state(s), from which the luminescence emission occurred. Thus, when they were excited by a 1040 nm laser, they need to absorb two photons simultaneously (Fig. 4c). To verify that the observed luminescence was induced by two-photon excitation, we measured series of emission intensities of TPABDFN-PSMA nanoparticles under the fs laser excitation with various powers. As shown in Fig. 4b, the two-photon fluorescence intensity was proportional to the square of the fs excitation intensity, confirming the characterization of a two-photon process [31]. The TPNIRFM image of TPABDFN-PSMA nanoparticles in

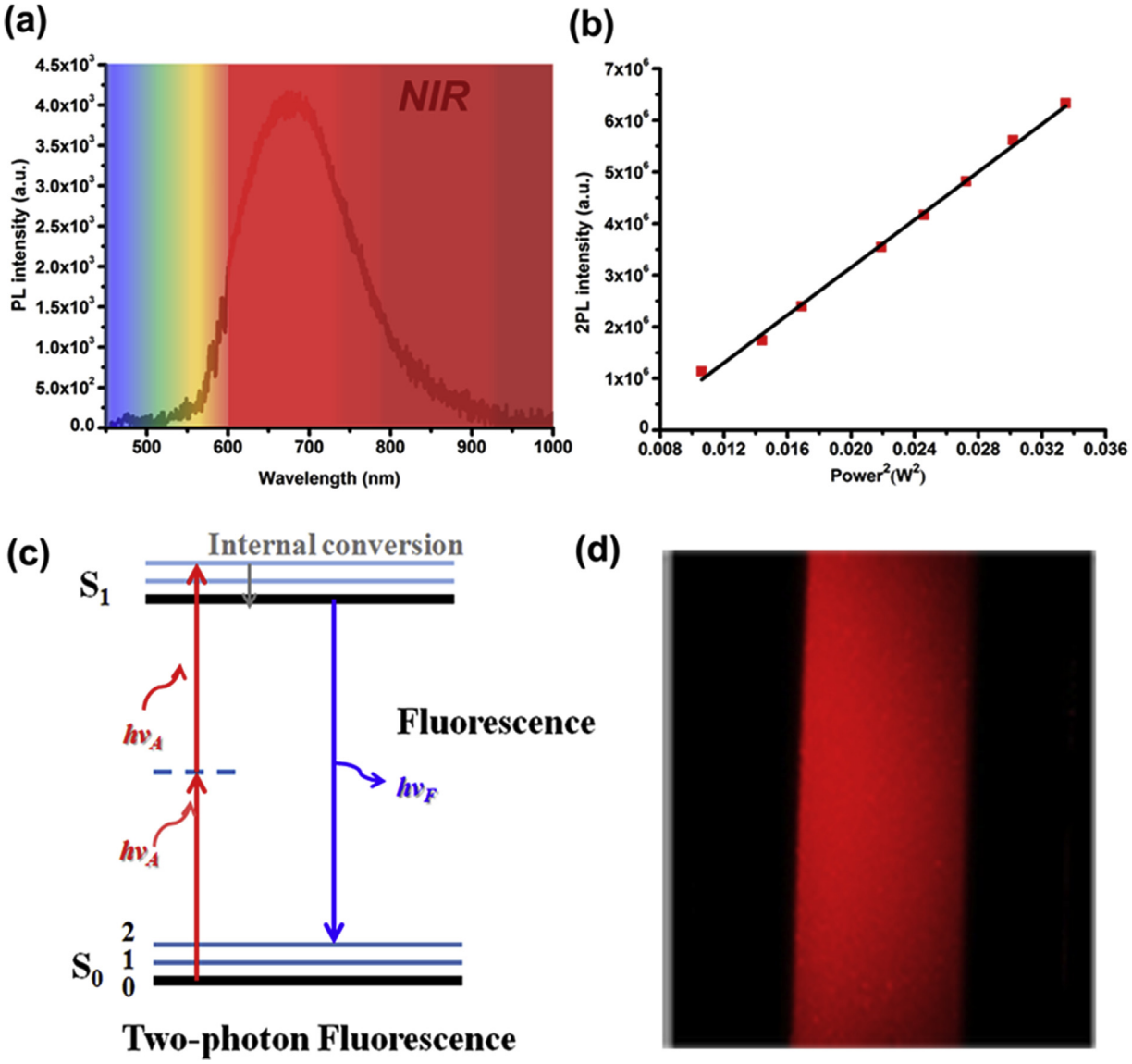

Fig. 4. (a) Two-photon fluorescence spectrum of TPABDFN-PSMA nanoparticles under the 1040 nm-fs excitation. (b) Square dependence of two-photon induced luminescence of TPABDFN-PSMA nanoparticles on excitation intensity of 1040 nm-fs laser. (c) Energy transition diagrams describing two-photon excited fluorescence. (d) A TPNIRFM image of TPABDFN-PSMA nanoparticles in capillary.

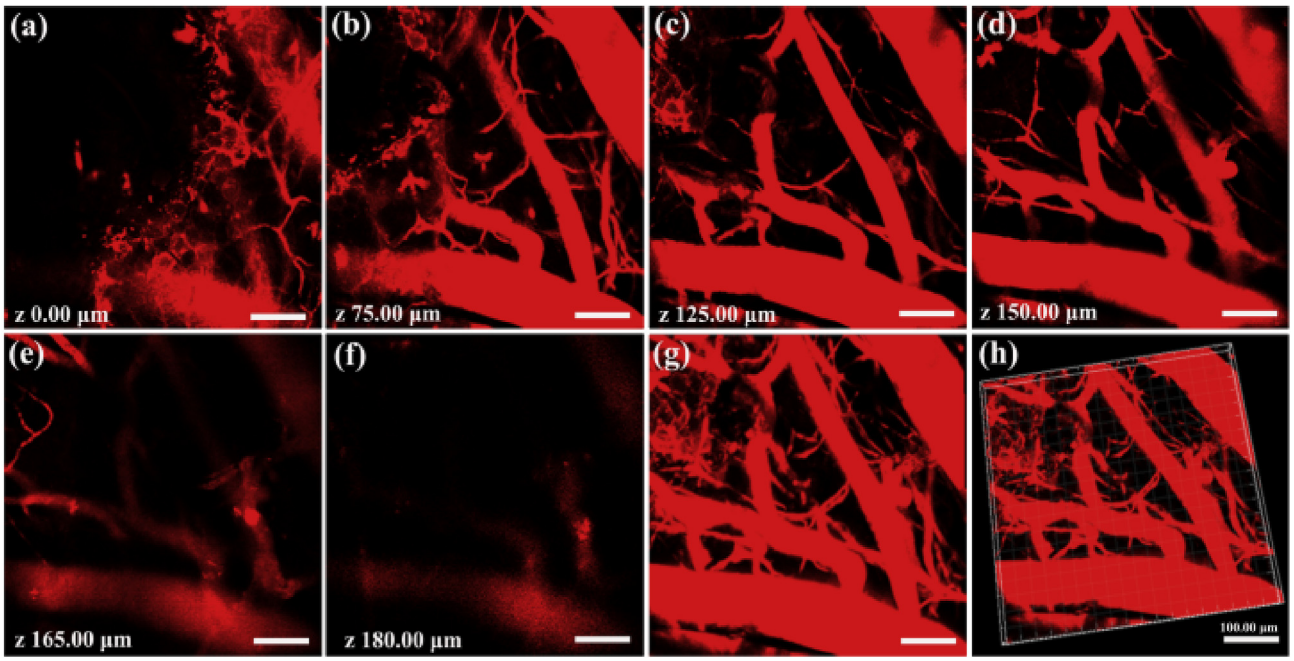

Fig. 5. TPNIRFM images of TPABDFN-PSMA-PEG nanoparticles stained ear blood vessels in the mouse, at various vertical depths: (a) 0 μm, (b) 75 μm, (c) 125 μm, (d) 150 μm, (e) 165 μm, and (f) 180 μm; (g) A stacked TPNIRFM image from a depth of 0 μm–180 μm. (h) A 3D reconstructed TPNIRFM image. Scale bar: 100 μm.

capillary was shown in Fig. 4d. Thanks to the distinct two-photon fluorescence of nanoparticles, the morphology of capillary could be clear visualized. Furthermore, the two-photon absorption cross-sections (δ) of TPABDFN-PSMA nanoparticles was measured, which was about 5.56×10^5 GM. It illustrated the nanoparticles possessed very distinct two-photon absorption effect, which was very helpful to the deep-tissue TPNIRFM imaging.

3.7. *In vivo* TPNIRFM imaging of TPABDFN-PSMA-PEG nanoparticles in blood vessels of a mouse ear

First, we used a mouse ear vessel model to examine the capability of TPABDFN-PSMA-PEG nanoparticles in *in vivo* TPNIRFM imaging. Fig. 5a–f showed the images of TPABDFN-PSMA-PEG nanoparticles at various depths of the mouse ear skin, under the 1040 nm-fs-excitation. Aside from the small capillaries located throughout the dermis, major veins and arteries located deeper within the dermis could also be observed. Fig. 5h showed a 3D reconstructed image of the blood vasculature network within a region of the ear dermis. In the control mouse (injected with 1 × PBS), no obvious autofluorescence from ear vessels could be observed even when the excitation power was very high (Fig. S18). Combining the above results, it could be confirmed that the TPNIRF signals detected from the ear blood vessels of mice, which were treated with the sample, were indeed from the TPABDFN-PSMA-PEG nanoparticles flowing in the blood vessels. TPABDFN-PSMA-PEG nanoparticles hold great promise to serve as an alternative contrast agent for intravital blood vasculature imaging.

Furthermore, we also used the mouse ear vessel model to examine the supersession of TPABDFN-PSMA-PEG nanoparticles inside the mouse body, based on the *in vivo* TPNIRFM imaging. Fig. S19 shows the imaging results of ear blood vessel of mice at various time points post TPABDFN-PSMA-PEG nanoparticles injection. 1 h after sample treatment, bright two-photon fluorescence was observed in the ear blood vessels of mouse (Fig. S19a). 6 h post the treatment, the two-photon fluorescence decreased in the blood vessels (Fig. S19b), due to the clearance of TPABDFN-PSMA-PEG over time. 12 h after sample injection, some weak two-photon fluorescence from TPABDFN-PSMA-PEG could still be detected (Fig. S19c). 24 h later, no luminescence signal could be observed from the blood vessels (Fig. S19d). The above results demonstrate that TPABDFN-PSMA-PEG nanoparticles could circulate in the mouse body for at least 12 h, which is very helpful to long-term *in vivo* imaging and tracing.

3.8. *In vivo* TPNIRFM imaging of TPABDFN-PSMA-PEG nanoparticles in blood vessels of a mouse brain

In vivo TPNIRFM imaging of mouse brain vessels was performed by using TPABDFN-PSMA-PEG nanoparticles. A cranial window surgery was performed on the brain of an ICR mouse (18 g. female), and 300 μL TPABDFN-PSMA-PEG nanoparticles in 1 × PBS (0.125 mg/mL) was then intravenously injected into the mouse. The surgery treated area of the brain was chosen for TPNIRFM imaging. Fig. 6a–h showed the TPNIRFM images of the mouse brain at various depths, under the 1040 nm fs excitation. Thanks to the two-photon fluorescence of TPABDFN-PSMA-PEG nanoparticles, the major blood vessels and smaller capillaries in the pia mater could be visualized clearly.

A stack image (Fig. 7a) was acquired when the step depth was set as 2 μm (2 μs/pixel, 512 × 512 pixels). Fig. 7b showed a 3D reconstructive TPNIRFM image of the blood vasculature network within a region of the mouse brain, and the imaging depth reached ~1200 μm, which was larger than that of any TPFM imaging performed on commercial systems. To the best of our knowledge, it was also the largest two-photon microscopic imaging depth by using 1040 nm (or nearby)-fs laser as the excitation source [32,33]. We attributed it to the deep penetration and good focusing capability of 1040 nm-fs excitation, as well as the low loss of NIR emission in biological tissues. In the control mouse (without the treatment of nanoparticles), no obvious autofluorescence from brain vessels could be detected even when the excitation power was very high (Fig. S20). These above experimental results demonstrated that TPNIRFM imaging of TPABDFN-PSMA-PEG

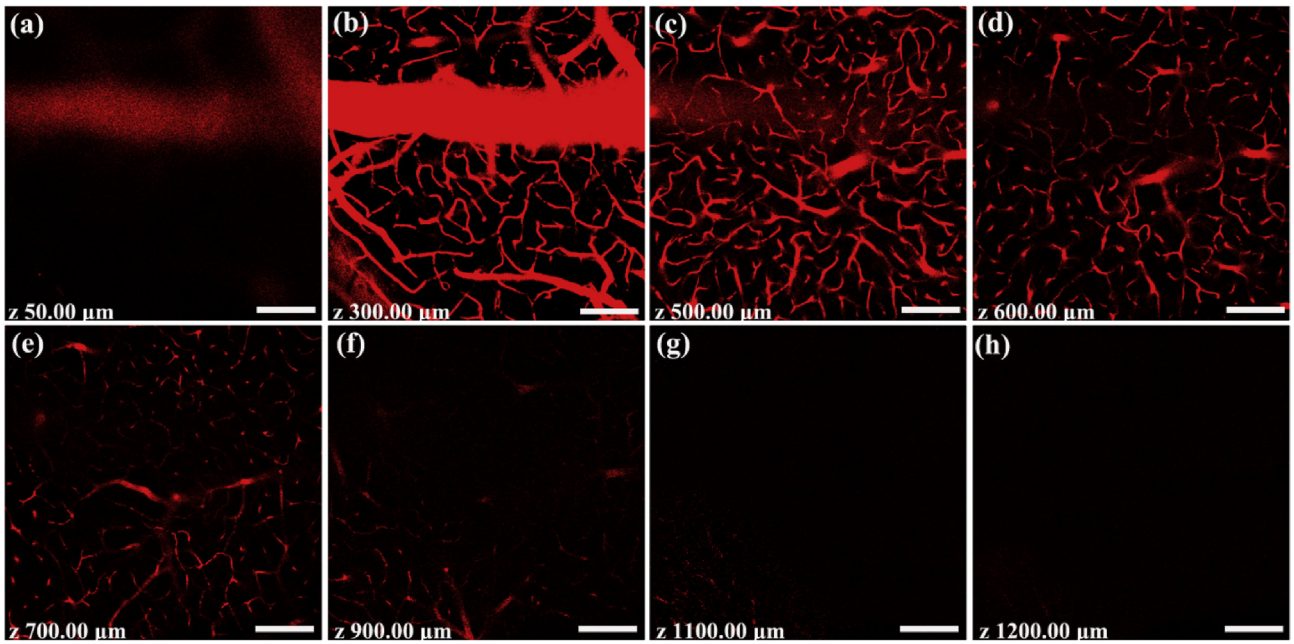

Fig. 6. TPNIRFM images of TPABDFN-PSMA-PEG nanoparticles stained brain blood vessels in the mouse at various depths: (a) 50 μm, (b) 300 μm, (c) 500 μm, (d) 600 μm, (e) 700 μm and (f) 900 μm (g) 1100 μm and (h) 1200 μm. Scale bar: 100 μm.

nanoparticles excited by 1040 nm fs laser is advantageous for high contrast and ultra-deep *in vivo* imaging.

4. Conclusion

In summary, an organic dye 2-(4-bromophenyl)-3-(4-(4-

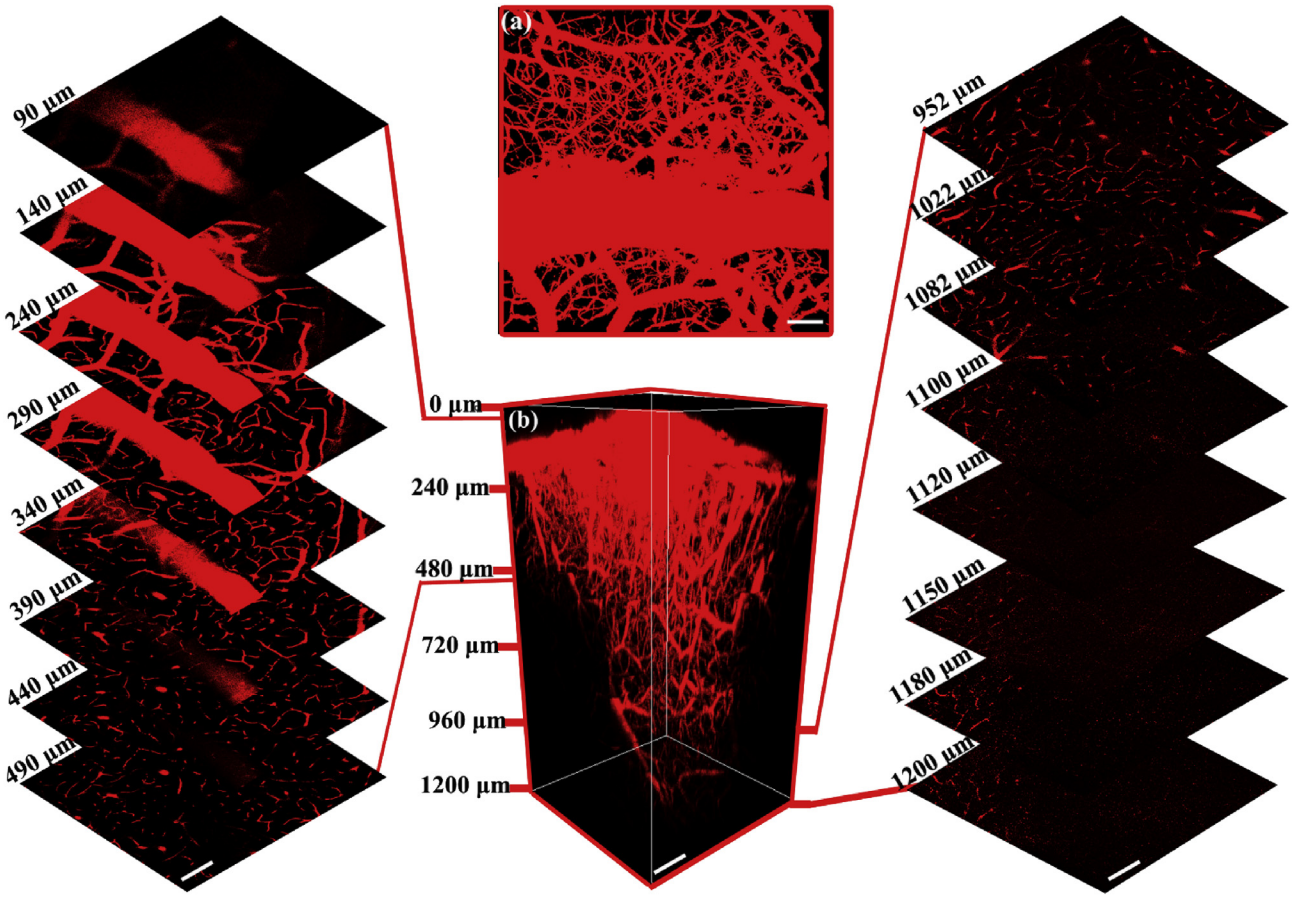

Fig. 7. (a) A stacked TPNIRFM image from a depth of 0 μm–1200 μm. (b) A 3D reconstructed TPNIRFM images of TPABDFN-PSMA-PEG nanoparticles stained brain blood vessels in the mouse. Scale bar: 100 μm.

(diphenylamino)styryl)phenyl) fumaronitrile (TPABDFN) with large two-photon absorption cross-section and bright NIR emission has been presented. By encapsulation with poly(styrene-*co*-maleic anhydride) (PSMA), TPABDFN-PSMA nanoparticles show high chemical and optical stability, large two-photon absorption (TPA) cross-section (5.56×10^5 GM), as well as bright NIR emission. mPEG-NH_2 is further grafted onto the nanoparticles, to afford good biocompatibility. TPABDFN-PSMA nanoparticles are utilized as fluorescent contrast agents for two-photon excited NIR microscopic imaging, under 1040 nm-femtosecond excitation. *In vivo* angiography of mice ear and brain is performed, and due to the deep penetration capability of both 1040 nm-excitation and NIR emission light, a very large imaging depth of 1200 μm was achieved. NIR emissive and biocompatible TPABDFN-PSMA nanoparticles have provided an effective platform for disease diagnosis and clinical therapies, where deep-tissue imaging is required.

Acknowledgements

This work was supported by National Basic Research Program of China (973 Program; 2013CB834704), the National Natural Science Foundation of China (61275190 and 81430010), the National High Technology Research and Development Program of China (863 Program; 2015AA020515), the Program of Zhejiang Leading Team of Science and Technology Innovation (2010R50007), and the Fundamental Research Funds for the Central Universities. Nuernisha Alifu is grateful to Mr. J. Q. Li in Thorlabs for his help in two-photon scanning microscope and Mr. K. Wu for his help in animal experiments.

Appendix A. Supplementary data

Supplementary data related to this article can be found at http://dx.doi.org/10.1016/j.dyepig.2017.04.017.

References

[1] Lakowicz JR. Principles of fluorescence spectroscopy. New York: Springer; 2006.
[2] Rust M, Bates JM, Zhuang XW. Sub-diffraction-limit imaging by stochastic optical reconstruction microscopy (STORM). Nat Methods 2006;3:793–5.
[3] Betzig E, Patterson GH, Sougrat R, Lindwasser OW, Olenych S, Bonifacino JS, et al. Imaging intracellular fluorescent proteins at nanometer resolution. Science 2006;313:1642–5.
[4] Axelrod D. Total internal reflection fluorescence microscopy in cell biology. Traffic 2001;2:764–74.
[5] Kobat D, Horton NG, Xu C. *In vivo* two-photon microscopy to 1.6-mm depth in mouse cortex. J Biomed Opt 2011;16:106014.
[6] Qian J, Wang D, Cai F, Zhan Q, Wang Y, He S. Photosensitizer encapsulated organically modified silica nanoparticles for direct two-photon photodynamic therapy and *in vivo* functional imaging. Biomaterials 2012;33:4851–60.
[7] Hong GS, Zou YP, Antaris AL, Diao S, Wu D, Cheng K, et al. Ultrafast fluorescence imaging *in vivo* with conjugated polymer fluorophores in the second near-infrared window. Nat Commun 2014;5:4206.
[8] Hinds S, Myrskog S, Levina L, Koleilat G, Yang J, Kelley SO, et al. NIR-emitting colloidal quantum dots having 26% luminescence quantum yield in buffer solution. J Am Chem Soc 2007;129:7218.
[9] Yong KT, Roy I, Ding H, Bergey EJ, Prasad PN. Biocompatible near-infrared quantum dots as ultrasensitive probes for long-term *in vivo* imaging applications. Small 2009;5:1997–2004.
[10] Liu Q, Sun Y, Yang T, Feng W, Li C, Li F. Sub-10 nm hexagonal lanthanide-doped $NaLuF_4$ upconversion nanocrystals for sensitive bioimaging *in vivo*. J Am Chem Soc 2011;133:17122–5.
[11] Xia A, Gao Y, Zhou J, Li C, Yang T, Wu D, et al. Core-shell $NaYF_4$:Yb^{3+},Tm^{3+}@Fe_xO_y nanocrystals for dual-modality t-2-enhanced magnetic resonance and NIR-to-NIR upconversion luminescent imaging of small-animal lymphatic node. Biomaterials 2011;32:7200–8.
[12] Dabbousi BO, Rodriguez-Viejo J, Mikulec FV, Heine JR, Mattoussi H, Ober R, et al. (CdSe)ZnS core-shell quantum dots: synthesis and Characterization of A Size series of highly luminescent nanocrystallites. J Phys Chem B 1997;101:9463–75.
[13] Shi L, Zhu C, He H, Zhu D, Zhang Z, Pang D, et al. Near-infrared Ag_2Se quantum dots with distinct absorption features and high fluorescence quantum yields. Rsc Adv 2016;6:38183–6.
[14] (a) Lovrić J, Cho SJ, Winnik FM, Maysinger D. Unmodified cadmium telluride quantum dots induce reactive oxygen species formation leading to multiple organelle damage and cell death. Chem Biol 2005;12:1227–34.
(b) Hardman RA. Toxicologic review of quantum dots: toxicity depends on physicochemical and environmental factors. Environ Health Perspect 2006;114:165–72.
[15] (a) Liu Z, Cai W, He L, Nakayama N, Chen K, Sun X, et al. *In vivo* biodistribution and highly efficient tumour targeting of carbon nanotubes in mice. Nat Nanotech 2007;2:47–52.
(b) Fitzpatrick JAJ, Andreko SK, Ernst LA, Waggoner AS, Ballou B, Bruchez MP. Long-term persistence and spectral blue shifting of quantum dots *in vivo*. Nano Lett 2009;9:2736–41.
[16] Gnanasammandhan MK, Idris NM, Bansal A, Huang K, Zhang Y. Near-ir photoactivation using mesoporous silica-coated $NaYF_4$: Yb, Er/Tm upconversion nanoparticles. Nat Protoc 2016;11:688–713.
[17] Han J, Xia H, Wu Y, Kong SN, Deivasigamani A, Xu R, et al. Single-layer MoS_2 nanosheet grafted upconversion nanoparticles for near-infrared fluorescence imaging-guided deep tissue cancer phototherapy. Nanoscale 2016;8:7861–5.
[18] Yu M, Li F, Chen Z, Hu H, Zhan C, Yang H, et al. Laser scanning upconversion luminescence microscopy for imaging cells labeled with rare-earth nanophosphors. Anal Chem 2009;81:930–5.
[19] Wang Y, Hu R, Xi W, Cai F, Wang S, Zhu Z, et al. Red emissive AIE nanodots with high two-photon absorption efficiency at 1040 nm for deep-tissue *in vivo* imaging. Biomed Opt Express 2015;6:3783–94.
[20] Shen XY, Yuan WZ, Liu Y, Zhao Q, Lu P, Ma Y, et al. Fumaronitrile-based fluorogen: red to near-infrared fluorescence, aggregation-induced emission, solvatochromism, and twisted intramolecular charge transfer. J Phys Chem C 2012;116:10541–7.
[21] Han X, Bai Q, Yao L, Liu H, Gao Y, Li J, et al. Highly efficient solid-state near-infrared emitting material based on triphenylamine and diphenylfumaronitrile with an EQE of 2.58% in nondoped organic light-emitting diode. Adv Funct Mater 2015;25:7521–9.
[22] Qian J, Wang D, Cai F, Peng L, Zhu Z, He H, et al. Observation of multiphoton-induced fluorescence from graphene oxide nanoparticles and applications *in vivo* functional bioimaging. Angew Chem Int Ed 2012;51:10570–5.
[23] Geng J, Goh CC, Tomczak N, Liu J, Liu R, Ma L, et al. Micelle/silica Co-protected conjugated polymer nanoparticles for two-photon excited brain vascular imaging. Chem Mater 2014;26:1874–80.
[24] Makarov NS, Drobizhev M, Rebane A. Two-photon absorption standards in the 550-1600 nm excitation wavelength range. Opt Express 2008;16:4029–47.
[25] Oulianov DA, Tomov IV, Dvornikov AS, Rentzepis PM. Observations on the measurement of two-photon absorption cross-section. Opt Commun 2001;191:235–43.
[26] He J, Xu B, Chen F, Xia H, Ye KL, Tian W. Aggregation-induced emission in the crystals of 9,10-distyrylanthracene derivatives: the essential role of restricted intramolecular torsion. J Phys Chem C 2009;113:9892–9.
[27] Xu B, He J, Dong Y, Chen F, Yu W, Tian W. Aggregation emission properties and self-assembly of conjugated oligocarbazoles. Chem Commun 2011;47:6602–6.
[28] Zhang J, Xu B, Chen J, Wang L, Tian W. Oligo(phenothiazine)s: twisted intramolecular charge transfer and aggregation-induced emission. J Phys Chem C 2013;117:23117–25.
[29] Zhang J, Xu B, Chen J, Ma S, Dong Y, Wang L, et al. An organic luminescent molecule: what will happen when the “butterflies” come together? Adv Mater 2014;26:739–45.
[30] Zhang X, Yu J, Wu C, Jin Y, Rong Y, Ye F, et al. Importance of having low-density functional groups for generating high-performance semiconducting polymer dots. ACS Nano 2012;6:5429–39.
[31] He GS, Zheng Q, Yong KT, Erogbogbo F, Swihart MT, Prasad PN. Two- and three-photon absorption and frequency upconverted emission of silicon quantum dots. Nano Lett 2008;8:2688–92.
[32] Perillo EP, McCracken JE, Fernée DC, Goldak JR, Medina FA, Miller DR, et al. Deep *in vivo* two-photon Microscopy with A Low cost custom built mode-locked 1060 nm fiber laser. Biomed Opt Express 2016;7:324–34.
[33] Wise FW. Femtosecond fiber lasers based on dissipative processes for nonlinear microscopy. IEEE J Sel Top Quant Electron 2012;18:1412–21.